# Reactive Multifunctional Template-Induced Preparation of Fe-N-Doped Mesoporous Carbon Microspheres Towards Highly Efficient Electrocatalysts for Oxygen Reduction

*Fan-Lu Meng, Zhong-Li Wang, Hai-Xia Zhong, Jun Wang, Jun-Min Yan, and Xin-Bo Zhang**

The oxygen reduction reaction (ORR) is generally the reaction that limits the efficiency of many electrochemical conversion and storage devices, including fuel cells and metal-air batteries, because of its intrinsically sluggish kinetics.[1,2] Although platinum and its alloys are traditionally known as the best ORR catalysts,[3] many critical problems, including the high cost, scarcity, low durability, crossover, and CO poisoning effects, still impede their large-scale practical application.[4] Iron-nitrogen-doped carbon (Fe-N-C) materials have been emerging as very promising noble-metal-free ORR catalysts,wherein the introduced Fe and N atoms could induce an uneven charge distribution and thus improve the $O_2$ adsorption and reduction.[5,6] Furthermore, by constructing mesoporous Fe-N-C materials the intrinsic advantages of mesopores (2–50 nm) and high specific surface areas in terms of high-flux mass transportation and efficient utilization of active catalytic sites could be exerted.[7,8] However, traditional methods of producing mesoporous materials highly rely on the use of mesoporous silica templates,[8e–g] whereby the employed silica templates can only be used as a hard template to build the mesoporous structure. This means that additional time-consuming and dangerous hydrofluoric acid or hot alkaline liquor treatment processes are necessary to remove the silica template. By using microspheres as the template, however, which generally have stable open frameworks compared to other mesoporous structures, the process results in reduced diffusion lengths and is very conducive to avoid aggregation on the electrode surface to ensure high efficiency of mass transfer.[7g] However, there are very few reports on the successful construction of high-performance mesoporous Fe-N-C microspheres as ORR catalysts. Furthermore, their synthesis still heavily relies on complex processes, combining monodispersed small silica spheres as the template to produce uniform mesopores, with impregnation of Fe and N precursors, and high-temperature carbonization treatment.[9] The ORR electrochemical performances of the thus-obtained mesoporous Fe-N-C microspheres was, however, still far from satisfying. This may partially be due to the fact that the physical mixture of N and Fe precursors and the silica template is not well qualified to control the uniform distribution towards a microstructure nor to guide the composition homogeneity of the resultant mesoporous Fe-N-C microspheres. Therefore, the development of a facile and effective strategy to synthesize well-shaped mesoporous Fe-N-C microspheres and exert their electrochemical performance toward ORR is highly desirable although very challenging.

Herein, an electrocatalyst consisting of Fe-N-doped mesoporous carbon microspheres (Fe-NMCSs) is for the first time synthesized using a facile in situ replication and polymerization strategy. Herein, the mesoporous ferroferric oxide ($Fe_3O_4$) microspheres are employed as multifunctional template–mesoporous structure-directing agent, as a source of $Fe^{3+}$ ions that are used as an oxidation agent for the polymerization of pyrrole, and especially as the precursor of Fe for the doping of Fe-NMCSs. This strategy highly improves the utilization and digestion of the templates, which thus eliminates the dangers related to the HF or hot alkaline liquor treatments that are needed to remove the hard template in conventional methods. Unexpectedly, the obtained Fe-NMCSs catalyst exhibited a superior ORR performance, including high activity, superior durability, and good tolerance to methanol in comparison to commercial Pt/C catalysts. The Fe-NMCSs can thus be successfully employed as a promising cathode catalyst both in real alkaline and proton fuel cells.

As presented in **Scheme 1**, the mesoporous $Fe_3O_4$ microspheres are firstly dispersed in deionized water by sonication and used as reactive multifunctional templates. Then, hexadecyltrimethylammonium bromide (CTAB), pyrrole monomers, and hydrochloric acid (HCl) solution are added in sequence, wherein HCl provides a strong acidic environment and CTAB helps with the dispersion. As $H^+$ and pyrrole monomers penetrate into the interior space of the mesoporous $Fe_3O_4$ microspheres, the $Fe^{3+}$ ions etched from the $Fe_3O_4$ act as oxidizer to the in situ polymerization of the pyrrole monomers. During polymerization, $Fe^{3+}$ ions are trapped inside the pores of the polypyrrole microspheres and subsequently used as Fe-doping source. Finally, the target Fe-NMCSs catalysts are obtained after carbonization of the Fe-modified polypyrrole mesoporous microspheres (Fe-PPy-MSs).

F.-L. Meng, Dr. Z.-L. Wang, H.-X. Zhong, J. Wang, Prof. X.-B. Zhang
State Key Laboratory of Rare Earth Resource Utilization
Changchun Institute of Applied Chemistry
Chinese Academy of Sciences
Changchun 130022, Jilin, P. R. China
E-mail: xbzhang@ciac.ac.cn
F.-L. Meng, Prof. J.-M. Yan
Key Laboratory of Automobile Materials
Ministry of Education and College of Materials Science and Engineering
Jilin University
Changchun 130012, Jilin, P. R. China
H.-X. Zhong, J. Wang
University of Chinese Academy of Sciences
Beijing 100049, P. R. China

DOI: 10.1002/adma.201602490

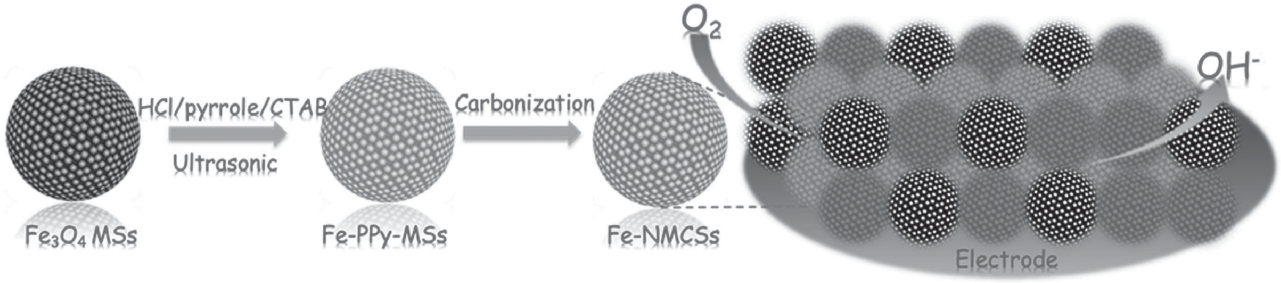


**Scheme 1.** Schematic representation of the preparation process of the Fe-NMCSs catalyst.

The morphology and microstructure of the as-synthesized Fe-NMCSs are characterized by field-emission scanning electron microscopy (FE-SEM) and transmission electron microscopy (TEM). As shown in **Figure 1**a and b, the $Fe_3O_4$ template retains its mesoporous microsphere structure, where the microspheres have a diameter of around 250 nm, and its crystalline structure can be identified as face-centered cubic $Fe_3O_4$ (Figure S1, Supporting Information, JCPDS card No. 19–629)[10] according to the X-ray diffraction (XRD) pattern. After reaction, the uniform Fe-PPy-MSs inherit the spherical structure of $Fe_3O_4$ but they had a rougher surface and increased diameter (ca. 500 nm), as can be seen in Figure 1c and d. From the XRD pattern of the Fe-PPY-MSs it can be seen that the main peaks of $Fe_3O_4$ disappeared, reflecting the complete conversion of oxide to polypyrrole polymer (Figure S1, Supporting Information). After pyrolysis, Fe-PPy-MSs is transformed to Fe-NMCSs. The XRD pattern of Fe-NMCSs displays two broad peaks with $2\theta$ values of 25° and 44° that can be indexed to carbon (002) and (101) diffractions, respectively (Figure S1, Supporting Information). No other diffraction peaks could be observed, indicating the absence of crystalline metallic Fe and/or Fe compounds (oxide, carbide, and/or nitride) in the Fe-NMCSs or the content is too low to be detected. That is well consistent with the TEM results, where we hardly observed any metal-containing nanoparticles (Figure S2a, inset, Supporting Information). The geometric characteristics of the Fe-NMCSs were almost exactly replicated from the microstructure of the Fe-PPy-MSs, although the diameter of the Fe-NMCSs was reduced to around 250 nm because of the decomposition of the PPy polymer during the calcination process (Figure 1e and f). This calcination process also produced abundant small pores over the microsphere among interconnected small particles (Figure 1e and f). It is worth noting that the Fe-NMCSs catalyst can be well dispersed without agglomeration (Figure S2, Supporting Information), contributing to a higher surface area and stable open frameworks on the electrode surface to ensure a high mass-transfer efficiency. The porous feature of the Fe-NMCSs was further confirmed by nitrogen adsorption–desorption isotherms. The isotherms of Fe-NMCSs were found to be typical type-IV isotherms, indicating the presence of mesopores (Figure 1g and h). The mesopore size distribution of the Fe-NMCSs displayed two peaks at 12.6 and 3.9 nm with an average pore width of 10.5 nm. The Fe-NMCSs also showed a high Brunauer–Emmett-Teller (BET) surface area (674 $m^2\ g^{-1}$) with a total pore volume of 0.71 $cm^3\ g^{-1}$. For comparison, we also prepared nitrogen-doped mesoporous carbon microspheres (NMCSs) and nitrogen carbon particles (NCPs) without Fe ions. Because of the similar synthesis process, the NMCSs and Fe-NMCSs had a similar mesoporous microsphere structure. The NCPs resulted from the pyrolysis of modified traditionally synthesized polypyrrole particles,[11] which hold irregular granular shapes and are seriously aggregated (Figure S3b,c, Supporting Information) with a surface area of 584 $m^2\ g^{-1}$ and average pore size of 4.1 nm (Figure S3d).

The composition and elemental distribution of the Fe-NMCSs catalyst was then analyzed using energy-dispersive X-ray spectroscopy (EDS). Typical EDS mapping analysis (Figure S4, Supporting Information) shows the uniform distribution of C, N, and Fe atoms in the Fe-NMCSs. The uniformity is believed to result from the in situ synthesis of the Fe-PPy-MSs. The porous structure with homogeneous nitrogen and iron species distribution provides more and easily accessible active sites, which will be beneficial for the electrochemical performance of the Fe-NMCSs catalyst. The nitrogen content in the Fe-NMCSs, NMCSs, and NCPs was measured to be 2.0%, 1.8%, and 4.2% by EDS, respectively, whereas the Fe content was too low to be quantified accurately by EDS (Table S1, Supporting Information). The Fe content was verified to be 0.50 at% by inductively coupled plasma optical emission spectrometry (ICP-OES). The chemical state of nitrogen in the Fe-NMCSs catalyst was investigated by X-ray photoelectron spectroscopy (XPS). The XPS N1s spectra could be deconvoluted into four peaks and attributed to the pyridinic-N (398.2 eV), pyrrolic-N (399.8 eV), quaternary-N (401 eV), and pyridinic-N-oxidized (402.1 eV) nitrogen atoms (**Figure 2**).[12] The N1s core-level spectrum of the Fe-PPy-MSs is dominated by a main peak at 399.2 eV assigned to neutral nitrogen atoms in the polymer (pyrrolic-N) (Figure S5, Supporting Information).[11a,c] The generation of different nitrogen chemical states is accompanied by a large decrease in the pyrrolic-N peak owing to the decomposition of the pyrrole ring in PPy-MSs, which happens at 600 °C, and the majority of the nitrogen in the pyrrole ring is depleted during the high-temperature pyrolysis.[13] Pyridinic-N and quaternary-N are the main nitrogen species in the Fe-NMCSs catalyst (**Figure 3**). Pyridinic-N (probably including Me-N) and graphitic-N are generally believed to contribute to the active sites for ORR.[14] The nitrogen species distribution of NMCSs is almost in agreement with that of the Fe-NMCSs (Figure 2c). However, the NCPs show a much higher quaternary-N content (Figure 2b and c). Figure 2d shows the Fe 2p spectrum. According to previous reports,[5e,14b] the peak at 711.3 eV suggests the presence of the chemical bonding between the Fe

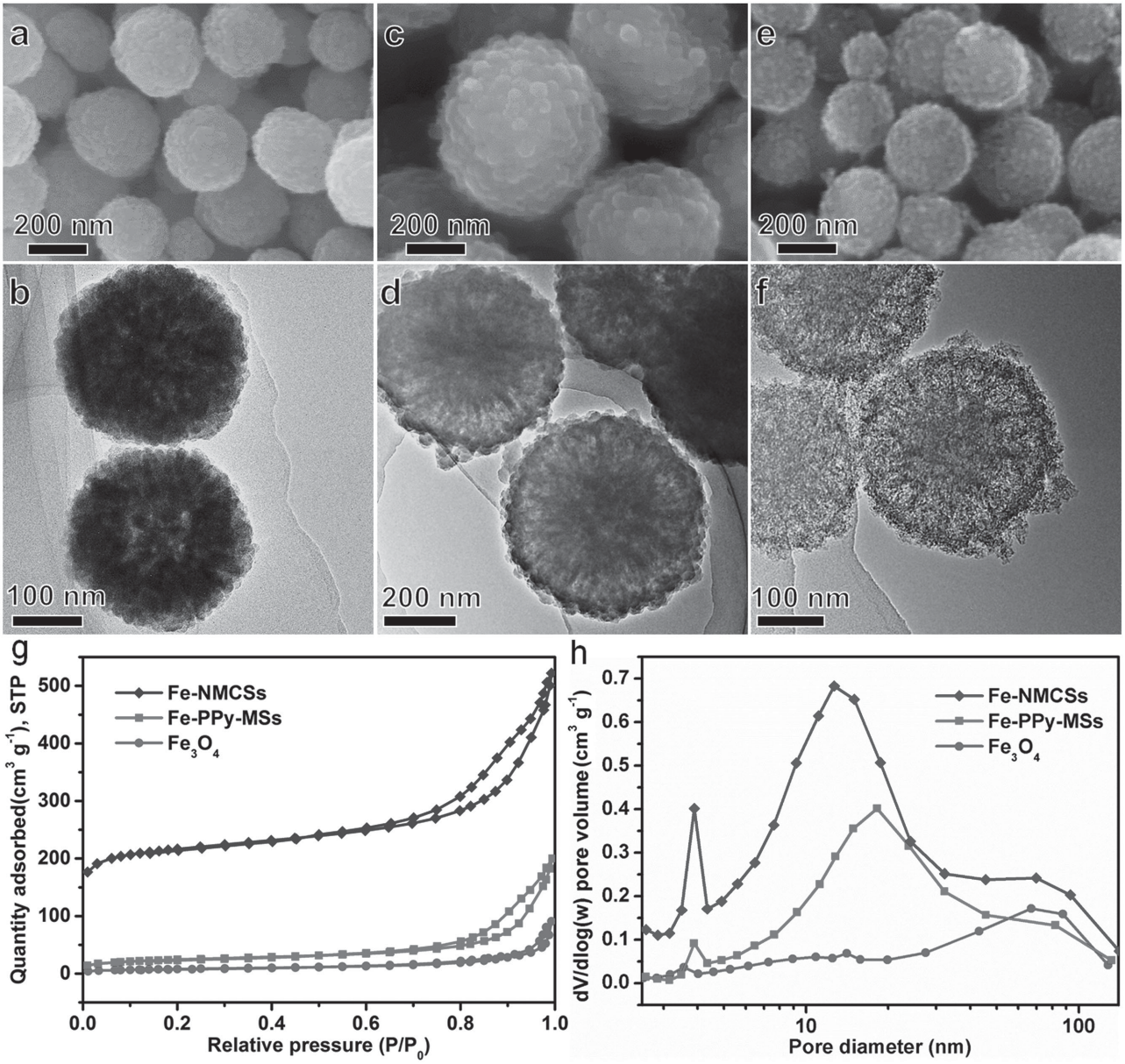


**Figure 1.** a, b) SEM and TEM images of mesoporous $Fe_3O_4$ microspheres. c, d) SEM and TEM images of Fe-PPy-MSs. e, f) SEM and TEM images of Fe-NMCSs. g) Nitrogen adsorption–desorption isotherms of Fe-NMCSs, Fe-PPy-MSs, and mesoporous $Fe_3O_4$ microspheres. h) Pore-size distributions of Fe-NMCSs, Fe-PPy-MSs, and mesoporous $Fe_3O_4$ microspheres.

and N moieties in the doped material. The peaks at 709.7 and 712.9 eV can be assigned to the binding energies of the $2p_{3/2}$ orbitals of $Fe^{2+}$ and $Fe^{3+}$ species, which might be related to different oxides. The peak at 708.2 eV may be related to metallic iron. For the $2p_{1/2}$ band, the peak at 723.4 eV can be attributed to the binding energy of $Fe^{2+}$. The peak at 717.2 eV is a satellite peak. According to earlier reports,[6e,14b,15] the metal ion center could promote initial $O_2$ adsorption and the adsorbed reaction intermediates thereby maximize the oxygen-reduction activity.

To investigate the ORR catalytic activities of the Fe-NMCSs samples, cyclic voltammetry (CV) experiments were performed in $N_2$- and $O_2$-saturated 0.1 M KOH solution at a scan rate of 50 mV $s^{-1}$. No obvious redox peak was observed for Fe-NMCSs in $N_2$-saturated electrolyte. In contrast, when the electrolyte was saturated with $O_2$, a well-defined cathodic peak clearly appeared at around 0.85 V (Figure S6, Supporting Information), which confirmed the electrocatalytic activity for the ORR. Rotating disk electrode (RDE) measurements were carried out to further evaluate the catalytic performance of the Fe-NMCSs. The Fe-NMCSs catalyst exhibited an onset potential of 1.027 V with a half-wave potential ($E_{1/2}$) of 0.86 V,[16] which is even better than that of commercial Pt/C catalyst (Figure 3a). In sharp contrast, the catalytic activity of the NMCSs catalyst was much worse compared to that of the Fe-NMCSs, even if they both held a similar structure and approximately the same nitrogen content

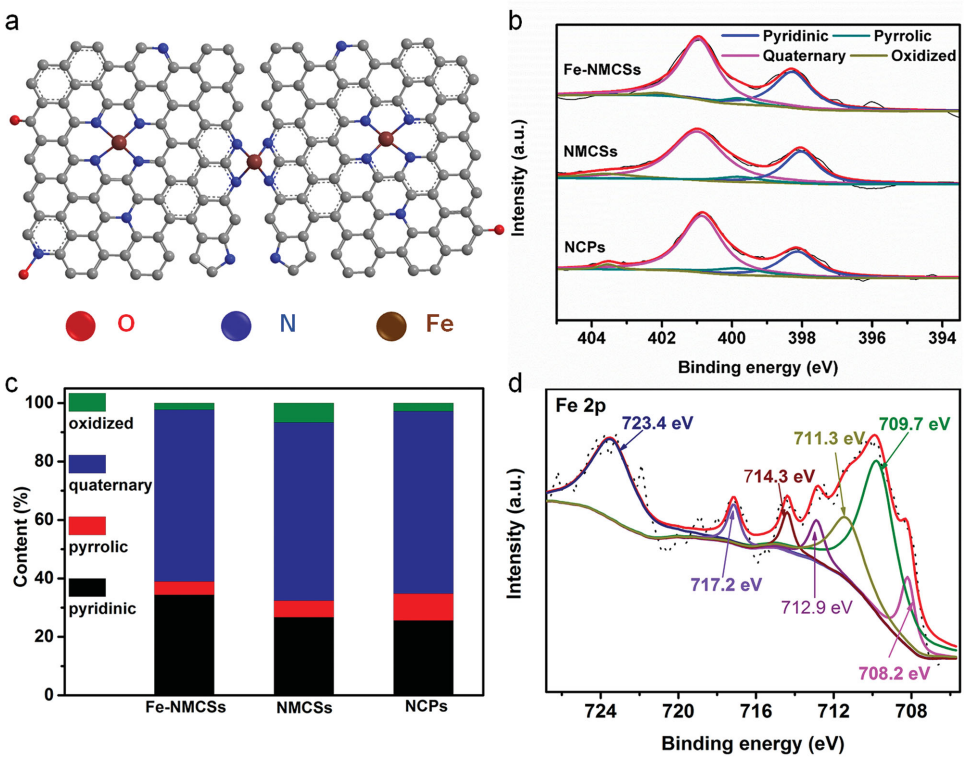


**Figure 2.** a) Schematic representation of nitrogen chemical states. b) N 1s XPS spectra of Fe-NMCSs, NMCSs, and NCPs. c) Relative ratios of the deconvoluted peak areas of the N 1s XPS spectra for Fe-NMCSs, NMCSs, and NCPs. d) The Fe 2p XPS spectra of Fe-NMCSs.

(with a mainly consistent nitrogen species distribution). This indicates that the existence of an Fe species plays a key part in the electrocatalytic activity. To identify the role of iron in the formation of active sites, we compared the ORR activity of Fe-NMCSs in 0.1 M KOH before and after adding 50 mM of cyanide ($CN^-$) ions. The ORR $E_{1/2}$ of the Fe-NMCSs catalyst decreased significantly by more than 100 mV, with a serious decrease in the diffusion-limiting current with the addition of $CN^-$ (Figure S8, Supporting Information), suggesting the formation of Fe-N*x* complexes. It is well known that $CN^-$ ions coordinate strongly to iron and poison the iron-centered catalytic sites for ORR.[1e] Furthermore, the enhanced mass transfer and larger surface area benefit from the mesoporous microsphere structure, which is clearly demonstrated by the higher ORR diffusion limiting current and half-wave potential of the NMCSs catalyst compared to that of the NCPs, even though the NCPs have a higher nitrogen content.

The RDE curves for ORR on the Fe-NMCSs electrode at various rotation speeds in $O_2$-saturated 0.1 M KOH are shown in Figure 3b. Koutecky–Levich (K–L) equations were used to analyze the kinetic parameters. The K–L plots (Figure 3b, inset) show excellent linearity and are parallel for Fe-NMCSs at various potentials. The according number of electrons transferred (*n*) was thus calculated to be an average value of 4.05 at potentials ranging from 0.3–0.6 V, suggesting that oxygen gas is reduced most likely through a direct four-electron pathway. However, the average *n* value for the NMCSs and NCPs catalysts were only 3.46 and 3.22, respectively (Figure S9, Supporting Information), indicating the existence of a less efficient two-electron pathway. The ORR involves a multi-electron transfer process in which $O_2$ can be directly converted into $OH^-$:

$$O_2 + 2H_2O + 4e^- \rightarrow 4OH^- \quad (1)$$

$O_2$ may also undergo two $2e^-$ processes to form $HO_2^-$ and then $OH^-$:

$$O_2 + H_2O + 2e^- \rightarrow HO_2^- + OH^- \quad (2a)$$

$$HO_2^- + H_2O + 2e^- \rightarrow 3OH^- \quad (2b)$$

A rotating ring disk electrode (RRDE) technique was employed to monitor the formation of peroxide and study the selectivity of the four-electron reduction of oxygen on the as-prepared Fe-NMCSs catalyst. The $HO_2^-$ yield (%) and the electron transfer number (*n*) are shown in Figure 3c,d. The $HO_2^-$ yield was less than 3.5% over the potential range from 0.2 to 0.8 V and the *n* ranged from 3.94 to 3.99, which is almost in keeping with the results from the K–L plots, and similar to those on Pt/C ($n = 4$), meaning that mainly a four-electron pathway occurs on the Fe-NMCSs. In contrast, when it comes to the NMCSs and NCPs, the $HO_2^-$ yield was much higher. Higher electron-transfer numbers, which imply a higher selectivity toward one-step oxygen reduction, are achieved with a combination of mesoporous microspheres and Fe species.

To evaluate the electrochemical stability of the Fe-NMCSs and monitor unwanted methanol crossover, chronoamperometric measurements were conducted (Figure 3e and f). After 25000 s, the commercial Pt/C catalyst suffered from 18.9% loss of current density, probably due to the loss and de-activation

ADVANCED MATERIALS
www.advmat.de

www.MaterialsViews.com

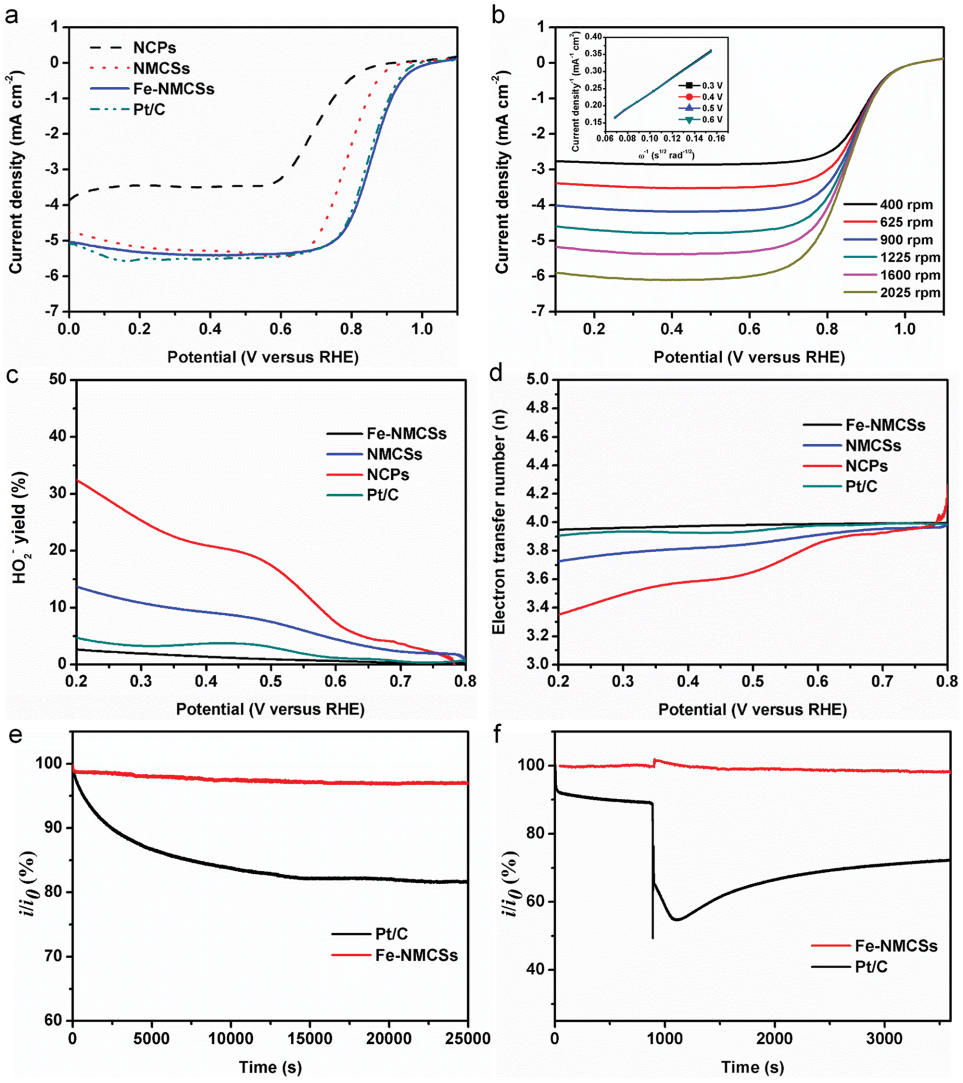


**Figure 3.** Electrochemical characterization of Fe-NMCSs in $O_2$-saturated 0.1 M KOH. a) RDE polarization plots of Fe-NMCSs, NMCSs, NCPs, and commercial Pt/C catalysts at a scan rate of 10 mV $s^{-1}$ and rotation speed of 1600 rpm. b) Voltammograms of Fe-NMCSs at various speeds at a scan rate of 10 mV $s^{-1}$; inset is the corresponding K–L plots at different potentials. c,d) Hydrogen peroxide yields (c) and electron-transfer numbers (d) of Fe-NMCSs, NMCSs, NCPs, and commercial Pt/C catalysts. e) Current-time chronoamperometric responses of Fe-NMCSs and Pt/C at 0.55 V (at a rotation speed of 1600 rpm) over 25000 s. f) Chronoamperometric responses of Fe-NMCSs and Pt/C upon the addition of 2% (*v*/*v*) methanol after about 900 s.

of Pt nanoparticles.[17] In sharp contrast, the Fe-NMCSs catalyst only exhibited a slight loss of about 2.8% in current density, indicating a superior durability of the Fe-NMCSs for ORR. This might be related to its stable open framework structure to provide various paths for mass transportation and avert the possible collapse of structure. After the injection of methanol, no significant change was observed in the ORR current density of the Fe-NMCSs, implying its great tolerance to the methanol crossover effect. In contrast, the ORR current density of the commercial Pt/C catalyst significantly decreased, because of the inherent vulnerability to methanol of the Pt electrocatalyst.[18]

The Fe-NMCSs catalyst also put up a competitive electrocatalytic performance for ORR in 0.1 M $HClO_4$ solution. A well-defined cathodic peak at around 0.68 V confirmed the electrocatalytic activity for ORR in acidic environment (Figure S10, Supporting Information). The polarization curves showed that the half-wave potential, $E_{1/2}$, of Fe-NMCSs was 59 mV more negative than that of Pt/C, and a similar limiting current density as that of Pt/C catalysts was achieved for the Fe-NMCSs catalyst, as displayed in **Figure 4**a. The $H_2O_2$ yield was below 6%, resulting in *n* of 3.92–3.94 in the measured potential range of 0.2 to 0.6 V, revealing a four-electron-pathway dominated ORR process (Figure 4c). $SCN^-$ also has a high affinity for Fe ions, and it is a good substitute for $CN^-$, as $CN^-$ tends to form the highly toxic HCN in acidic electrolytes. The study of Qiang Wang[8d] and co-workers confirmed this, where they used $SCN^-$ to identify the active sites. In 0.1 M $HClO_4$ solution, after adding 5 mM of $SCN^-$, the negative shift of the $E_{1/2}$ clearly indicates that the active sites of the Fe-NMCSs catalyst contain Fe (Figure S12, Supporting Information). We carried out accelerated durability tests by cycling the catalyst between 0.55 and 0.95 V at 100 mV $s^{-1}$ under oxygen atmosphere to assess the

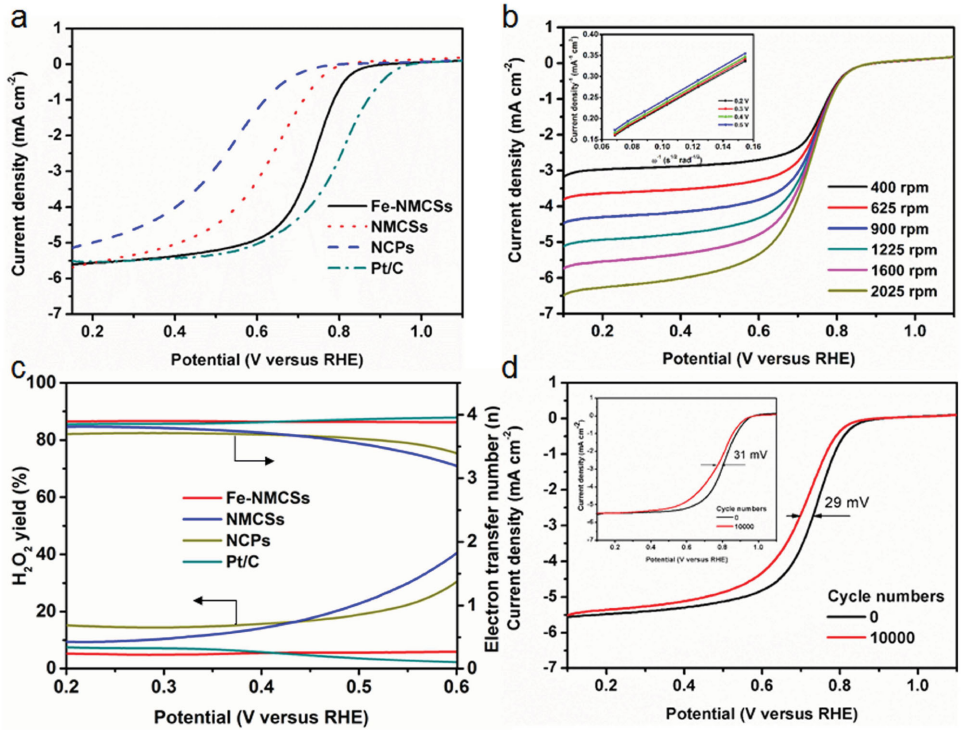


**Figure 4.** Electrochemical characterization of Fe-NMCSs in $O_2$-saturated 0.1 M $HClO_4$. a) RDE polarization plots of Fe-NMCSs, NMCSs, NCPs, and commercial Pt/C catalysts at a scan rate of 10 mV $s^{-1}$ and rotation speed of 1600 rpm. b) Voltammograms of Fe-NMCSs at various speeds at a scan rate of 10 mV $s^{-1}$; the inset shows the corresponding K–L plots at different potentials. c) Hydrogen peroxide yields and electron-transfer numbers ($n$) of Fe-NMCSs, NMCSs, NCPs, and commercial Pt/C catalysts at various potentials based on RRDE data. d) RDE polarization plots of Fe-NMCSs for ORR before and after 10000 cycles (inset for commercial Pt/C).

durability of the Fe-NMCSs catalyst. The negative shift in the half-wave potential $E_{1/2}$ after 10000 cycles for Fe-NMCSs was only 29 mV, which is slightly lower than that of Pt/C (31 mV), suggesting the excellent durability of the Fe-NMCSs catalyst in acidic medium (Figure 4d). Cyclic voltammetry was performed to test the effect of possible methanol crossover. The almost unchanged ORR peak current for the Fe-NMCSs compared to that of Pt/C (Figure S13, Supporting Information) suggests its high electrocatalytic selectivity for the ORR with a strong tolerance for methanol crossover. It is obvious that the Fe-NMCSs show a much higher onset and half-wave potential in alkaline medium. According to earlier reports for Fe-N-C materials,[6e] the stability of ferrous-hydroperoxyl adducts formed during oxygen reduction plays a very critical role and is seriously influenced by the hydrogen peroxide intermediate. In alkaline media, the $HO_2^-$ promotes the formation of stabilized adducts. However, this stabilization can be destroyed by the protonated nature of the hydrogen peroxide intermediate ($H_2O_2$) in acidic media, which leads to a higher overpotential for the ORR to further reduce $H_2O_2$.

Moving forward to practical applications, **Figure 5** shows the alkaline-exchange membrane fuel cell (AEMFC) and proton-exchange membrane fuel cell (PEMFC) performance of the Fe-NMCSs and Pt/C. The open-circuit voltage (OCV) of Fe-NMCSs was 1.07 V with a peak power density of 506 mW $cm^{-2}$, which is higher than that of 1.05 V and 438 mW $cm^{-2}$ for the

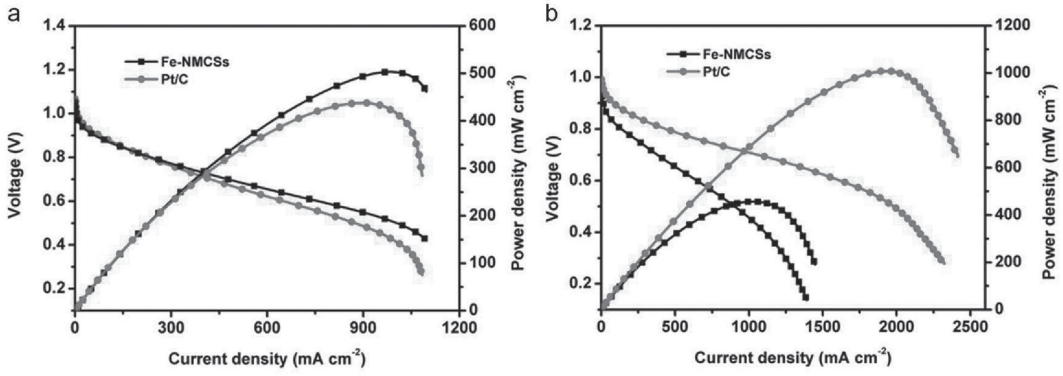


**Figure 5.** a,b) The cell voltage and power density of AEMFCs (a) and PEMFCs (b) with Fe-NMCSs and commercial Pt/C (40 wt%) as cathodes.

Pt/C catalyst in the AEMFC. In the PEMFC, the OCV values of Fe-NMCSs and Pt/C were 0.96 and 1.01 V, respectively. The peak power densities of the Fe-NMCSs and Pt/C were 463 mW $cm^{-2}$ and 1008 mW $cm^{-2}$. Although the performance of our mesoporous catalyst was lower than that of Pt/C, it is still competitive as compared to other non-noble catalysts. The above results reveal that the Fe-NMCSs can be successfully employed as a promising cathode catalyst in fuel cells. It should be noted that these preliminary fuel cell results could be further improved after optimizing the MEA assembly and the fuel-cell testing conditions (work still in progress in our group).

In summary, to take advantage of the high catalytic activity of Fe-N-C and the fast mass transport in mesoporous microsphere structures, a novel in situ replication and polymerization strategy has been developed to fabricate novel Fe-NMCSs, wherein the $Fe_3O_4$ mesoporous microspheres were employed as the multifunctional template – mesoporous structure-directing agent, as the source of $Fe^{3+}$ ions as oxidation agent for the polymerization of pyrrole, and as the Fe precursor for the Fe doping of Fe-NMCSs. Unexpectedly, compared to a commercial Pt/C catalyst, the obtained Fe-NMCSs catalyst demonstrated excellent electrocatalytic performance in terms of higher catalytic activity, selectivity, and durability for ORR in alkaline media, and a comparable activity to Pt/C in acidic medium. Especially, the Fe-NMCSs can be successfully employed as a promising cathode catalyst both in alkaline and proton fuel cells. This can be attributed to the open framework structure of the mesoporous microspheres, as well as the effective Fe doping. The developed synthesis strategy to tailor the size and structure of Fe-N doped mesoporous carbon can be easily extended to other systems for broad applications, including supercapacitors and carbon dioxide adsorption.

## Supporting Information

Supporting Information is available from the Wiley Online Library or from the author.

## Acknowledgements

This work is financially supported by 100 Talents Programme of the Chinese Academy of Sciences, National Program on Key Basic Research Project of China (973 Program, Grant No. 2012CB215500), Foundation for Innovative Research Groups of the National Natural Science Foundation of China (Grant No. 20921002), National Natural Science Foundation of China (Grant No. 21101147), and the Jilin Province Science and Technology Development Program (Grant No. 20100102 and 20116008).

Received: May 10, 2016
Revised: June 1, 2016
Published online: July 4, 2016

[1] a) M. K. Debe, *Nature* **2012**, *486*, 43; b) F. Y. Cheng, J. Chen, *Chem. Soc. Rev.* **2012**, *41*, 2172; c) F. Y. Cheng, J. Shen, B. Peng, Y. D. Pan, Z. L. Tao, J. Chen, *Nat. Chem.* **2011**, *3*, 79; d) G. Wu, K. L. More, C. M. Johnston, P. Zelenay, *Science* **2011**, *332*, 443; e) Y. G. Li, W. Zhou, H. L. Wang, L. M. Xie, Y. Y. Liang, F. Wei, J. C. Idrobo, S. J. Pennycook, H. J. Dai, *Nat. Nanotech.* **2012**, *7*, 394; f) J. Wang, K. Wang, F. B. Wang, X. H. Xia, *Nat. Commun.* **2014**, *5*, 5285.

[2] a) Y. Bing, H. Liu, L. Zhang, D. Ghosh, J. Zhang, *Chem. Soc. Rev.* **2010**, *39*, 2184; b) H. A. Gasteiger, J. E. Panels, S. G. Yan, *J. Power Sources* **2004**, *127*, 162; c) C. Sealy, *Mater. Today* **2008**, *11*, 65; d) D. S. Geng, Y. Chen, Y. G. Chen, Y. L. Li, R. Y. Li, X. L. Sun, S. Y. Ye, S. Knights, *Energy Environ. Sci.* **2011**, *4*, 760.

[3] a) V. R. Stamenkovic, B. Fowler, B. S. Mun, G. F. Wang, P. N. Ross, C. A. Lucas, N. M. Marković, *Science* **2007**, *315*, 493; b) J. Zhang, K. Sasaki, E. Sutter, R. R. Adzic, *Science* **2007**, *315*, 220; c) J. Greeley, I. E. L. Stephens, A. S. Bondarenko, T. P. Johansson, H. A. Hansen, T. F. Jaramillo, J. Rossmeisl, I. Chorkendorff, J. K. Nørskov, *Nat. Chem.* **2009**, *1*, 552; d) Z. W. Chen, M. Waje, W. Z. Li, Y. S. Yan, *Angew. Chem. Int. Ed.* **2007**, *46*, 4060; e) J. B. Wu, J. L. Zhang, Z. M. Peng, S. C. Yang, F. T. Wagner, H. Yang, *J. Am. Chem. Soc.* **2010**, *132*, 4984; f) Y. Liu, H. H. Wu, M. Li, J. J. Yin, Z. H. Nie, *Nanoscale* **2014**, *6*, 11904.

[4] a) L. M. Dai, *Acc. Chem. Res.* **2012**, *46*, 31; b) A. C. Chen, P. Holt-Hindle, *Chem. Rev.* **2010**, *110*, 3767; c) H. A. Gasteiger, S. S. Kocha, B. Sompalli, F. T. Wagner, *Appl. Catal. B: Environ.* **2005**, *56*, 9.

[5] a) K. P. Gong, F. Du, Z. H. Xia, M. Durstock, L. M. Dai, *Science* **2009**, *323*, 760; b) Y. Y. Liang, Y. G. Li, H. L. Wang, J. G. Zhou, J. Wang, T. Regier, H. J. Dai, *Nat. Mater.* **2011**, *10*, 780; c) J. Liu, X. J. Sun, P. Song, Y. W. Zhang, W. Xing, W. L. Xu, *Adv. Mater.* **2013**, *25*, 6879; d) W. Yang, T. P. Fellinger, M. Antonietti, *J. Am. Chem. Soc.* **2011**, *133*, 206; e) G. Wu, Z. W. Chen, K. Artyushkova, F. H. Garzon, P. Zelenay, *ECS Trans.* **2008**, *16*, 159.

[6] a) F. Charreteur, F. Jaouen, S. Ruggeri, J. P. Dodelet, *Electrochim. Acta* **2008**, *53*, 2925; b) J. Y. Choi, R. S. Hsu, Z. W. Chen, *J. Phys. Chem. C* **2010**, *114*, 8048; c) M. Lefèvre, E. Proietti, F. Jaouen, J. P. Dodelet, *Science* **2009**, *324*, 71; d) D. Zhao, J. L. Shui, C. Chen, X. Q. Chen, B. M. Reprogle, D. P. Wang, D. J. Liu, *Chem. Sci.* **2012**, *3*, 3200; e) N. Ramaswamy, U. Tylus, Q. Jia, S. Mukerjee, *J. Am. Chem. Soc.* **2013**, *135*, 15443.

[7] a) R. L. Liu, D. Q. Wu, X. L. Feng, K. Müllen, *Angew. Chem. Int. Ed.* **2010**, *49*, 2565; b) W. Yang, T.-P. Fellinger, M. Antonietti, *J. Am. Chem. Soc.* **2011**, *133*, 206; c) J. Liang, Y. Jiao, M. Jaroniec, S. Z. Qiao, *Angew. Chem. Int. Ed.* **2012**, *51*, 11496; d) J. Liang, Y. Zheng, J. Chen, J. Liu, D. Hulicova-Jurcakova, M. Jaroniec, S. Z. Qiao, *Angew. Chem. Int. Ed.* **2012**, *51*, 3892; e) J. W. Lu, P. Zhang, A. Li, F. L. Su, T. Wang, Y. Liu, J. L. Gong, *Chem. Commun.* **2013**, *49*, 5817; f) D. Yang, Z. Y. Lu, X. H. Rui, X. Huang, H. Li, J. X. Zhu, W. Y. Zhang, Y. M. Lam, H. H. Hng, H. Zhang, Q. Y. Yan, *Angew. Chem. Int. Ed.* **2014**, *53*, 9352; g) Z. K. Sun, Y. Liu, B. Li, J. Wei, M. H. Wang, Q. Yue, Y. H. Deng, S. Kaliaguine, D. Y. Zhao, *ACS Nano* **2013**, *7*, 8706.

[8] a) H. W. Liang, W. Wei, Z. S. Wu, X. L. Feng, K. Müllen, *J. Am. Chem. Soc.* **2013**, *135*, 16002; b) A. G. Kong, B. Dong, X. F. Zhu, Y. Y. Kong, J. L. Zhang, Y. K. Shan, *Chem. Eur. J.* **2013**, *19*, 16170; c) J. K. Dombrovskis, H. Y. Jeong, K. Fossum, O. Terasaki, A. E. C. Palmqvist, *Chem. Mater.* **2013**, *25*, 856; d) Q. Wang, Z. Y. Zhou, Y. J. Lai, Y. You, J. G. Liu, X. L. Wu, E. Terefe, C. Chen, L. Song, M. Rauf, N. Tian, S. G. Sun, *J. Am. Chem. Soc.* **2014**, *136*, 10882; e) A. G. Kong, Y. Y. Kong, X. F. Zhu, Z. Han, Y. K. Shan, *Carbon* **2014**, *78*, 49; f) A. G. Kong, X. F. Zhu, Z. Han, Y. Y. Yu, Y. B. Zhang, B. Dong, Y. K. Shan, *ACS Catal.* **2014**, *4*, 1793; g) J. Y. Cheon, T. Y. Kim, Y. M. Choi, H. Y. Jeong, M. G. Kim, Y. J. Sa, J. Kim, Z. H. Lee, T. H. Yang, K. J. Kwon, O. Terasaki, G. G. Park, R. R. Adzic, S. H. Joo, *Sci. Rep.* **2013**, *3*, 15.

[9] a) H. S. Liu, Z. Shi, J. L. Zhang, L. Zhang, J. J. Zhang, *J. Mater. Chem.* **2009**, *19*, 468; b) L. Zhang, J. Kim, E. Dy, S. Ban, K. Tsay, H. Kawai, Z. Shi, J. J. Zhang, *Electrochim. Acta* **2013**, *108*, 480.

[10] H. Deng, X. L. Li, Q. Peng, X. Wang, J. P. Chen, Y. D. Li, *Angew. Chem. Int. Ed.* **2005**, *44*, 2782.

[11] a) A. Morozan, P. Jegou, S. Campidelli, S. Palacin, B. Jousselme, *Chem. Commun.* **2012**, *48*, 4627; b) M. Sevilla, P. Valle-Vigón, A. B. Fuertes, *Adv. Funct. Mater.* **2011**, *21*, 2781; c) L. Wei, M. Sevilla, A. B. Fuertes, R. Mokaya, G. Yushin, *Adv. Funct. Mater.* **2012**, *22*, 827; d) X. X. Yuan, X. L. Ding, C. Y Wang, Z. F. Ma, *Energy Environ. Sci.* **2013**, *6*, 1105.

[12] Z. H. Sheng, L. Shao, J. J. Chen, W. J. Bao, F. B. Wang, X. H. Xia, *ACS Nano* **2011**, *5*, 4350.

[13] J. Z. Wang, S. L. Chou, J. Chen, S. Y. Chew, G. X. Wang, K. Konstantinov, J. Wu, S. X. Dou, H. K. Liu, *Electrochem. Commun.* **2008**, *10*, 1781.

[14] a) K. Parvez, S. B. Yang, Y. Hernandez, A. Winter, A. Turchanin, X. L. Feng, K. Müllen, *ACS Nano* **2012**, *6*, 9541; b) Y. Zhao, K. Watanabe, K. Hashimoto, *J. Am. Chem. Soc.* **2012**, *134*, 19528; c) W. Ding, Z. D. Wei, S. G. Chen, X. Q. Qi, T. Yang, J. S. Hu, D. Wang, L. J. Wan, S. F. Alvi, L. Li, *Angew. Chem.* **2013**, *125*, 11971.

[15] a) G. Lalande, R. Côté, G. Tamizhmani, D. Guay, J. P. Dodelet, L. Dignard-Bailey, L. T. Weng, P. Bertrand, *Electrochim. Acta* **1995**, *40*, 2635; b) T. Okada, M. Gokita, M. Yuasa, I. Sekine, *J. Electrochem. Soc.* **1998**, *145*, 15; c) G. Liu, X. Li, P. Ganesan, B. N. Popov, *Appl. Catal. B-Environ.* **2009**, *93*, 156.

[16] H. D. Sha, X. X. Yuan, L. Li, Z. Ma, Z. F. Ma, L. Zhang, J. J. Zhang, *J. Power Sources* **2014**, *255*, 76.

[17] a) P. J. Ferreira, G. J. La, O. Y. Shao-Horn, D. Morgan, R. Makharia, S. Kocha, H. A. Gasteiger, *J. Electrochem. Soc.* **2005**, *152*, A2256; b) R. Srivastava, P. Mani, N. Hahn, P. Strasser, *Angew. Chem.* **2007**, *119*, 9146.

[18] Z. H. Wen, J. Liu, J. H. Li, *Adv. Mater.* **2008**, *20*, 743.